Supplementary Information

Graphene Schottky Varactor Diodes for High-Performance Photodetection

Adi Levi[*1,2], Moshe Kirshner[*1,2], Ofer Sinai[1,2], Eldad Peretz[1,2], Ohad Meshulam[1,2], Arnab Ghosh[1,2], Noam Gotlib[1,2], Chen Stern[1,2], Shaofan Yuan[3], Fengnian Xia[3], and Doron Naveh[1,2†]

[1] Faculty of Engineering, Bar-Ilan University, Ramat-Gan, Israel, 52900

[2] Institute for Nanotechnology and Advanced Materials, Bar-Ilan University, Ramat-Gan, Israel, 52900

3 Department of Electrical Engineering, Yale University, New Haven CT 06511, USA

Additional Details on Varactor Diodes

CVD graphene was characterized by Raman spectroscopy after transfer to silicon wafers and after device fabrication. Typical Raman spectrum of the graphene is shown in **Error! Reference source not found.**. Logarithmic scale *I-V* is shown in Fig. S2, where the recorded dark current at 50 mV is 1 nA. Contact resistance in diodes is not well defined due to the nonlinear I-V transfer of the device. Here, transfer length modulation method was applied with respect to the device contact area. The *I-V* curves were measured at room temperature on devices with varying contact area and the transfer curves were fitted to the general formula: $I = Ae^{\alpha V}$. We note that the resistivity of graphene is very small as compared to contact impedance and therefore the device *I-V* is practically independent from channel length. The statistical distribution of the coefficient α was analyzed per contact area of devices as shown in **Figure S2**. We assess that α is independent from contact area as sampled from a set of 47 devices. Therefore, the *I-V* is

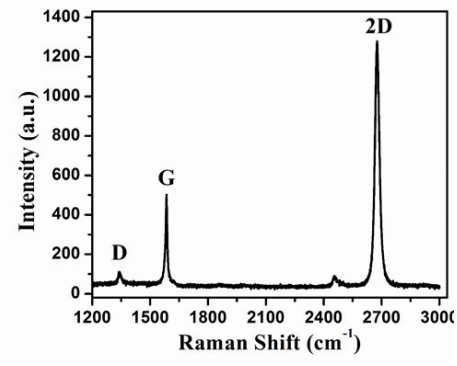

Figure S1. Raman spectrum acquired from a device CVD graphene channel.

dominated by the contact width and the current flow is from the contact edge to the graphene rather than through the entire contact area [1].

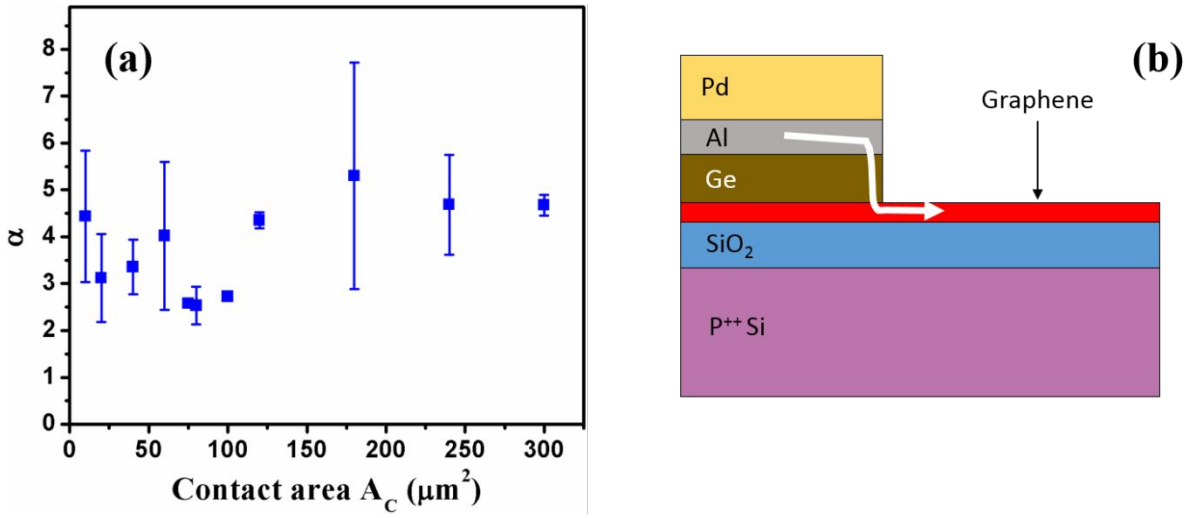

Figure S2. Exponential parameter of the diodes I-V as function of the device contact area (a) and the graphically illustrated edge contact.

We infer from **Figure S2** that the α parameter is independent from contact area and is highly sensitive to process variations. We observe clustering of the α values among devices metallized together at the same batches and attribute such clustering to small variations in the deposition of contacts.

Noise Equivalent Power

Current noise spectral density (**Figure S4**) was measured by the Fourier transform of current sampled at a DC bias of 0 mV and 100 mV for 10 seconds at a sampling rate of 6.45 kHz. . NEP is defined as the ratio of the current spectral density to the responsivity: $NEP = \frac{S_i}{R}$, where S_i is the current noise spectral density (in A $Hz^{-1/2}$) of the device and S_i is defined as

$$S_i(f) = \lim_{T\to\infty} \frac{1}{\sqrt{T}} \sqrt{\left| \int_{-T/2}^{T/2} I(t) e^{-2\pi i f t} dt \right|^2} \qquad \text{S1}$$

Here the average responsivity value is 100 mA/W and the measured noise spectral density is shown in **Figure S3**.

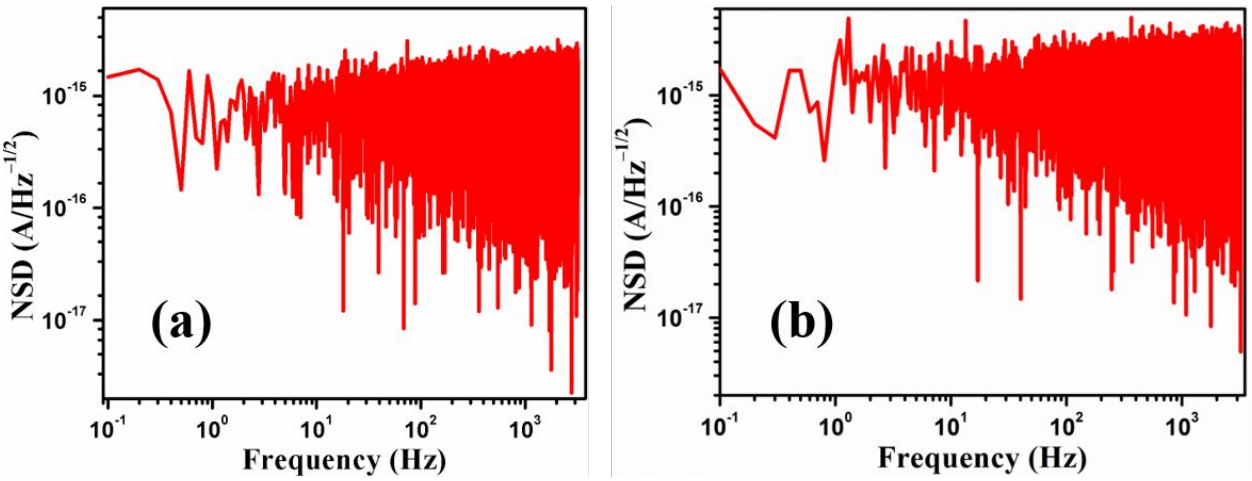

Figure S3. Noise spectral density as a fucntion of frequency at (a) 0 mV and (b) 100 mV.

Device Modeling

The measured capacitance and resistance of a varactor is shown in **Figure S4** below. For device modelling we assumed the circuit model of **Figure S5** and the measured capacitance and resistance. Within this model, device contacts are modeled as parallel variable capacitor and resistor, while the graphene channel as a parallel capacitor – inductor\resistor. The actual device impedance is obtained from C-V measurements in the form of $Z = Re\{Z\} + jIm\{Z\}$. Circuit components values were then fitted to the related model with transfer function $= \frac{C_q(R_g + jwL_g)}{C_q + R_g + jwL_g} + \frac{2R_p}{1 + jwR_pC_P}$, in such a way that value for the expression $|(Re\{Z\} + jIm\{Z\}) - (Re\{TF\} + jIm\{TF\})|$ is minimized. Here, the model output C_p and R_p are the device parallel capacitance and parallel resistance respectively. We have assigned the graphene resistance, R_g, the kinetic inductivity, L_g [2], and quantum capacitance, C_q [3], values of 500Ω, 1 pH and 1 pF, respectively.

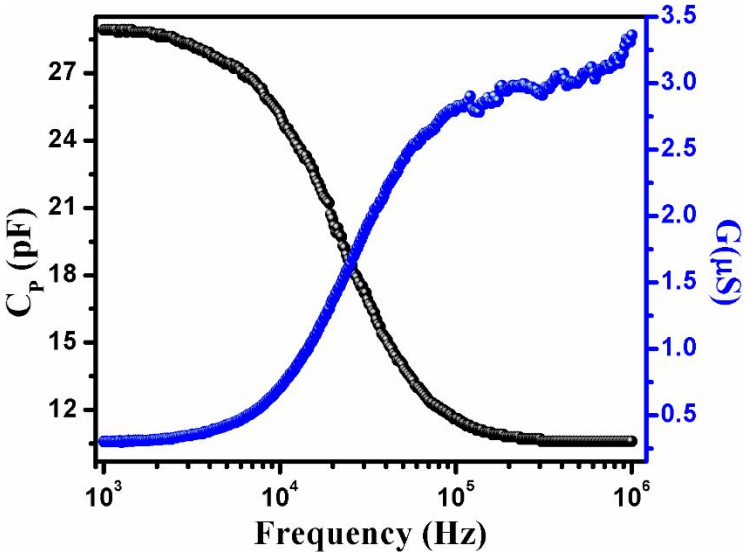

Figure S4. Device contact capacitance (black) and conductance (blue) as a function of frequency.

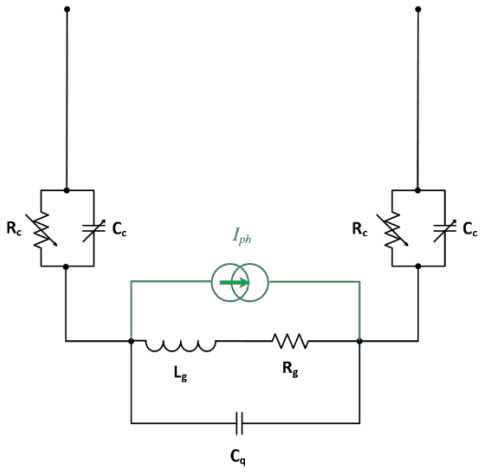

Figure S5. Schematic of circiut design of the presented varactor device.

Time-Dependent Photocurrent Measurements

Photocurrent was measured on a varactor diode without applying bias on it using Keysight CX3324A Device Current Waveform Analyzer (see inset of **Figure 2c**), by shining laser light modulated at a particular frequency *f* on the device. The (root mean square) amplitude of the recorded photocurrent

$I^{ph}\left(t_1 \ldots t_N\right)$, was then calculated using the relation $A(f)=\sqrt{\frac{1}{N}\sum_{j=1}^{N}\left|I_j^{ph}\right|^2}$. Finally, the relative amplitude was taken as $\eta(f)=\frac{A(f)}{A(f_1)}$ and presened as blue dots in **Figure 2c**.

Spatial Distribution of Photocurrent

In addition to the measurements conducted with large beam diameter (presented in manuscript), photocurrent mapping (**Figure S6**) were collected at 10 kHz modulation of focused laser beam (532 nm). At zero applied bias (**Figure S6a**) most of the photocurrent is collected from the vicinity of the electrodes, owing to the band bending profile of the device and corresponding to a PTE effect (see inset of the photocurrent profile along the device channel as indicated by white dash-dot mark.

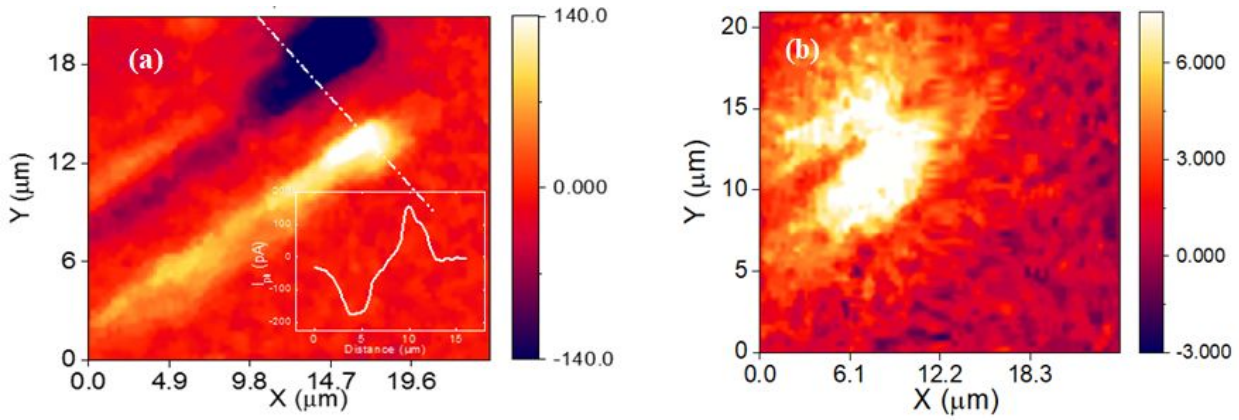

Figure S6. (a) Photocurrent map (pA units) acquired with focused laser beam at zero applied voltage showing the spatial distribution of photocurrent (inset: cross section along white dash-dot) and (b) mapping with applied bias of 1V (photocurrent in units of nA).

At a bias of 1V (**Figure S6b**), the photocurrent changes character – corresponding to the voltage induced slope in electrochemical potential along the device channel. Here the map is showing that the entire device area is active and that photocurrent is increased by an order of magnitude relative to unbiased device – and yet the dark current is very small relative to Ohmic photodetectors at 1V (see **Figure 1c**).

References

1. Xia, F.; Mueller, T.; Lin, Y.-m.; Valdes-Garcia, A.; Avouris, P., Ultrafast graphene photodetector. *Nature Nanotechnology* **2009,** *4* (12), 839.
2. Dae-Young, J.; Kook Joo, L.; Moonil, K.; Dong Chul, K.; Hyun-Jong, C.; Yun-Sung, W.; Sunae, S., Radio-Frequency Electrical Characteristics of Single Layer Graphene. *Japanese Journal of Applied Physics* **2009,** *48* (9R), 091601.
3. Xia, J.; Chen, F.; Li, J.; Tao, N., Measurement of the quantum capacitance of graphene. *Nature Nanotechnology* **2009,** *4*, 505.